Development of Design Procedures for Flexural Applications of Textile Composite Systems Based on Tension Stiffening Models

Barzin Mobasher[1]

Summary: The Aveston Copper and Kelly (ACK) Method has been routinely used in estimating the efficiency of the bond between the textile and cementitious matrix. This method however has a limited applicability due to the simplifying assumptions such as perfect bond. A numerical model for simulation of tensile behavior of reinforced cement-based composites is presented to capture the inefficiency of the bond mechanisms. In this approach the role of interface properties which are instrumental in the simulation of the tensile response is investigated. The model simulates the tension stiffening effect of cracked matrix, and evolution of crack spacing in tensile members. Independent experimental results obtained from literature are used to verify the model and develop composite tensile stress strain response using alkali resistant (AR) glass textile reinforced concrete.

The composite stress strain response is then used with a bilinear representation of the composite obtained from the tensile stiffening model. The closed form and simplified equations for representation of flexural response are obtained and used for both back-calculation and also design. A method based on the average moment-curvature relationship in the structural design and analysis of one way and two way flexural elements using yield line analysis approaches is proposed. This comprehensive approach directly shows the interrelation of fundamental materials characterization techniques with simplified design equations for further utilization of textile reinforced concrete materials.

[1] Professor, School of Sustainable Engineering and the Built Environment, Civil, Environmental, and Sustainable Engineering Program Arizona State University, Tempe, AZ 85287-5306

1 Introduction

The field of Textile Reinforced Concrete (TRC) has led the development of novel cement based materials with a significant degree of strength, ductility, and versatility [1,2]. With as much as one order of magnitude higher strength and two orders of magnitude higher in ductility than fiber reinforced concrete (FRC), TRC's development has utilized innovative fabrics, matrices, and manufacturing processes. A variety of fiber and fabric systems such as Alkali resistant (AR) glass fibers, polypropelene (PE), polyethylene (PE), and Poly Vinyl Alcohol (PVA) have been utilized [3,4]. Mechanical properties of the composites under uniaxial tensile, flexural, and shear tests indicate superior performance such as tensile strength as high as 25 MPa, and strain capacity of 1-8%. As compared to the conventional FRC materials, the fracture toughness is increased by as much as two orders of magnitude. The dominant toughening mechanisms in these systems are attributed to matrix cracking, ply delamination, and crack deflection mechanisms as studied by means of fluorescent microscopy, scanning electron microscopy.

Classes of strain-softening and hardening FRC are discussed by Naaman and Reinhardt [5]. Unlike FRC that fracture localization occurs immediately after the first crack is formed, distribution of cracking throughout the specimen in strain hardening cement composites (SHCC) is facilitated by the fiber bridging mechanism. Since a substantial amount of energy is required to further extend existing cracks, secondary cracks form. Single crack localization is therefore shifted to multiple distributed cracking mechanisms, leading to macroscopic pseudo-strain hardening behaviors as shown in Figure 1. When used as continuous reinforcement in cement matrices, the enhanced mechanical bond strength presented by the textiles result in a composite with strain hardening and multiple cracking behavior.

Since TRC materials exhibit the characteristics of Strain hardening materials (SHCC), they are well-suited for applications that may eliminate conventional reinforcement or for the structures in seismic regions where high ductility is desired [6]. In addition, strain hardening materials offer fatigue and impact resistance and are attractive for use in industrial structures, highways, bridges, earthquake, hurricane, and high wind loading conditions. The design and implementation of these systems requires the use within the strain-hardening range that is attributed to multiple cracking under tensile stresses. The post-crack response extends over a large strain range, and is modeled using a reduced stiffness. The simulation of reduced stiffness may be based on either empirical approaches obtained from experimental data [7], or gradual debonding of textiles using analytical debonding models [8].

In order to use TRC materials, fundamental approaches for tensile and flexural design are needed. This paper addresses methods to predict moment-rotation capacity integrated with a general template for predicting load deformation performance. Two examples of analysis and design of various structural systems are used to demonstrate the calculation steps.

The Aveston Cooper and Kelly model (ACK Model) addresses the increased strain capacity of the matrix and the multiple cracking mechanism in the presence of fibers in unidirectional composites [9]. This method however does not address the tension stiffening effect defined as the ability of the uncracked segments in between the two parallel cracks to carry tensile force. A majority of tension stiffening models in the literature either don't take into account the gradual transition of bond-slip mechanism or simplify it to a linear interfacial model.

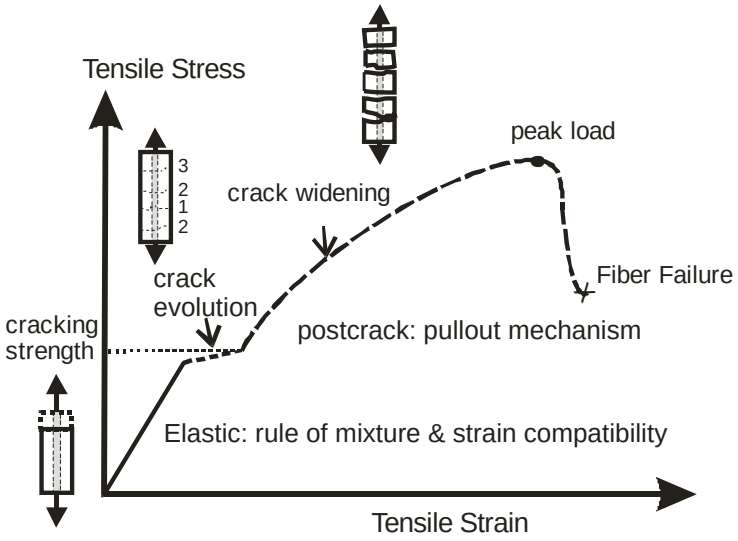

Fig. 1: Tensile response of a Strain hardening fiber cement based composite.

1.1 Tension stiffening model

The finite difference tension stiffening model developed by Soranakom and Mobasher [10,11,12,13] simulates the crack spacing and stress-strain response of SHCC materials under static and dynamic loads. Based on the finite difference method, the model takes into account non-linear bond slip model. The individual component failure criterion as presented for a continuous textile reinforced composite in Figure 2, are defined by three distinct mechanisms: matrix strength cracking criterion, interface bond-slip characteristics, and tensile stress-strain of the continuous fibers.

In this model a cracked tension specimen is idealized as a series of 1-D segments consisting of fiber, matrix, and interface elements. As the load on the composite increases such that the cracking stress of the matrix is reached, cracked planes form sequentially. The load at the cracked planes is solely carried by the longitudinal fibers by means of interface elements. The individual segments continue to transfer the load through the intact fibers at cracked locations. An iterative solution algorithm based on nonlinear analysis enforces that load-deformation response follows the material constitutive laws. Once the slip distributions are solved the corresponding stress and strain responses are identified.

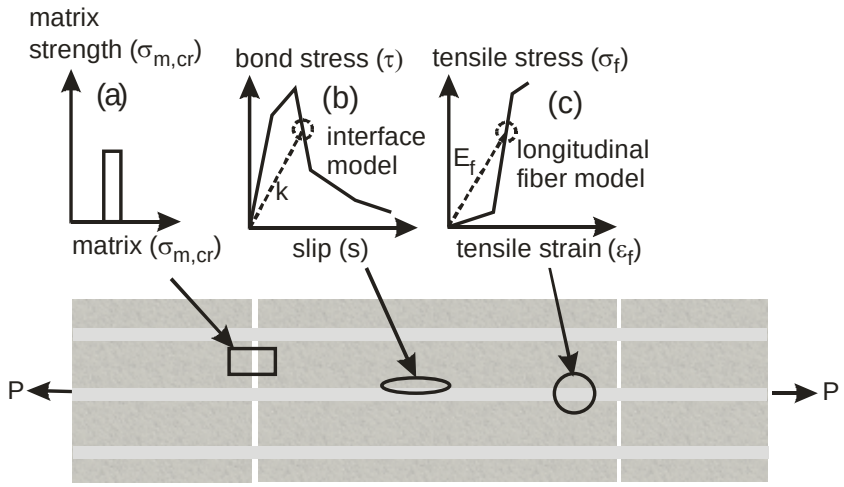

Fig. 2: Schematic representation of three distinct mechanisms in TRC: (a) matrix strength cracking (b) interface bond-slip characteristics and (c) tensile stress-strain of the continuous fibers.

The matrix is treated as brittle with no strain-softening with its cracking strength defined as $\sigma_{m,cr}$ as shown in Figure 2(a). The second characteristic parameter is the bond between fiber and matrix, described by a generalized free form bond stress $\tau = \tau(s)$ expressed as function of slip (s) (Figure 2(b)). Multi-linear segments define the pre and post-peak behaviors of the bond characteristics. At each load step, a secant modulus k enforces the local bond stress and slip at each node in the finite difference model to follow the prescribed bond-slip relation. The third aspect (Figure 2(c)) addresses fiber properties.

The equilibrium equations are derived from free body diagrams of the nodes and expressed as coefficient and the unknown variable slip (s), defined as the relative difference between the elongation of the continuous fibers and matrix. A finite length between two consecutive nodes i and i+1 along the longitudinal x-axis is used. The embedded length L is discretized into ‘‘n’’ nodes with equal spacing of “h” as shown in Figure 3a through 3c. The bond stress is assumed constant over the small spacing h for each node within each linear domain. At the left end force in the fiber is imposed to be zero, simulating stress free condition, implying that the fiber strain or derivative of slip vanishes. At the right end the nodal slip is prescribed incrementally, simulating displacement control. As the loading progresses, the part of the fiber that slips out of the matrix has no frictional bond resistance; thus, fiber elongation is the only term in that section. The extruding part can be easily implemented by checking the amount of slip versus the embedded length of each node. If the slip is greater than the embedded length, zero bond stress is applied to that node.

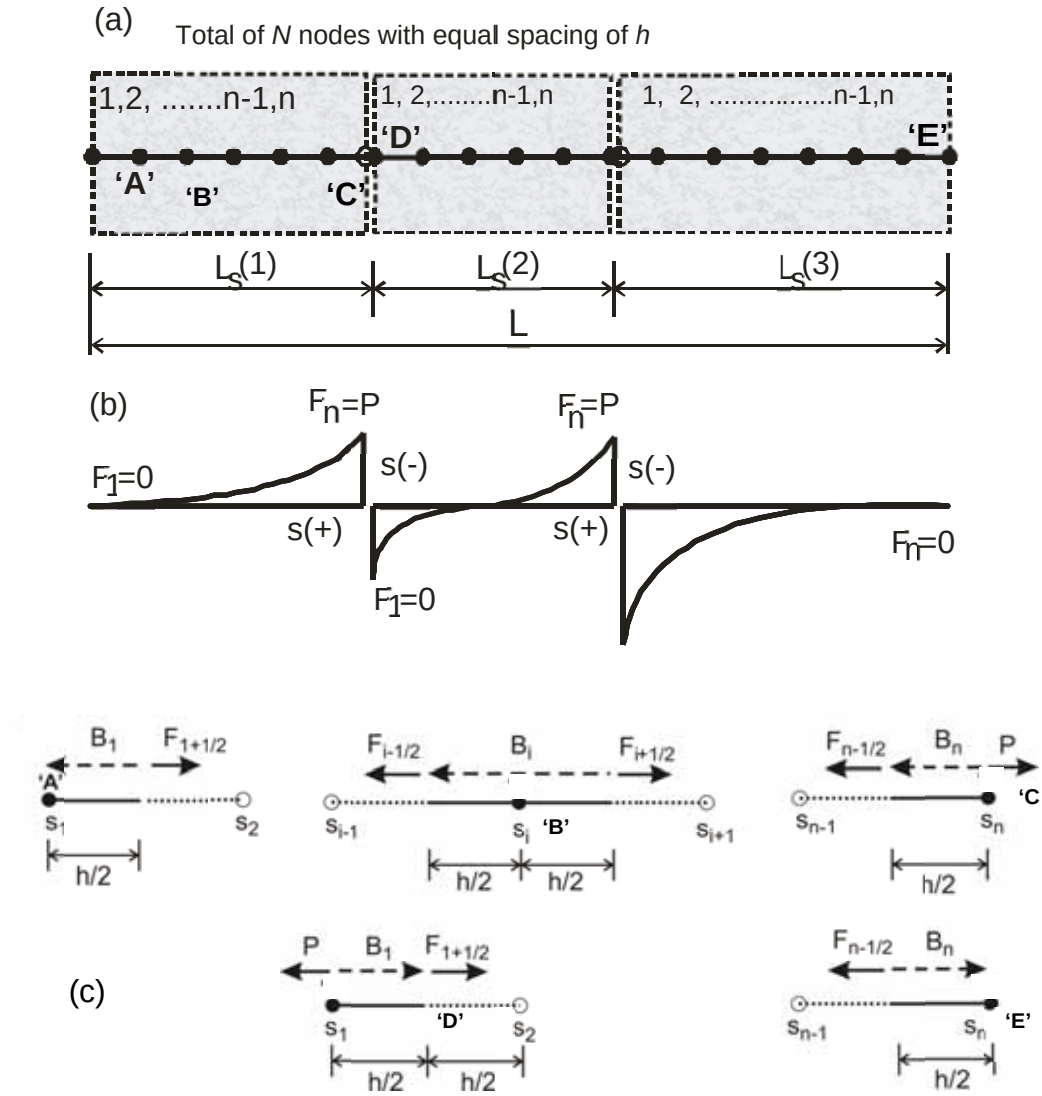

Fig. 3: Finite difference model: (a) discretized pull-out model, (b) Convention for slip and boundary conditions for force in fiber and (c) free body diagram of five representative nodes labeled as "A"- "E".

Both deterministic and stochastic crack patterns can be used. Either uniform matrix strengths with predetermined sequential equidistant cracking locations can be specified, or random matrix strengths at nodes along the length may be generated and used as local cracking criterion. A fiber efficiency factor is introduced to take into account the imperfect nature of the bond and inability of the fiber stiffness to be utilized within the test. This efficiency factor can be directly related to the measurements on inner and outside sleeve bond characteristics [14].

The pullout model is shown in Figure 4(a) using available experimental data addressing single fiber or textile systems [15]. Figure 4(b) represents both the fiber and interface model used in the simulation. While the applied load is less than the first cracking limit, elastic behavior is assumed and tensile response is calculated by means of the rule of mixtures. As the strength criterion of matrix is met, the sample is divided into two parts, each segment is modeled as a pull-out problem and solved independently. As the load increases, additional cracks form at locations as the strength criterion is satisfied and the process repeated. The cracked specimen is thus represented by a number of independently solved pull-out segments that represent the entire specimen. The analysis terminates as the stress in yarn reaches its ultimate tensile strength or a solution is not found due to slip instability (very large slip values).

It is observed from Figure 5(a) that by decreasing the values of efficiency of the interfacial bond η the total strain of the composite increases up to a point that the fiber starts to fracture. Fiber failure occurs when η equals 0.3. An efficiency factor of 0.6 corresponds with the ultimate strain of approximately 1.5% (close to experimental results). The crack spacing continues to extend to smaller values due to significant debonding and slip when the efficiency factor η decreases.

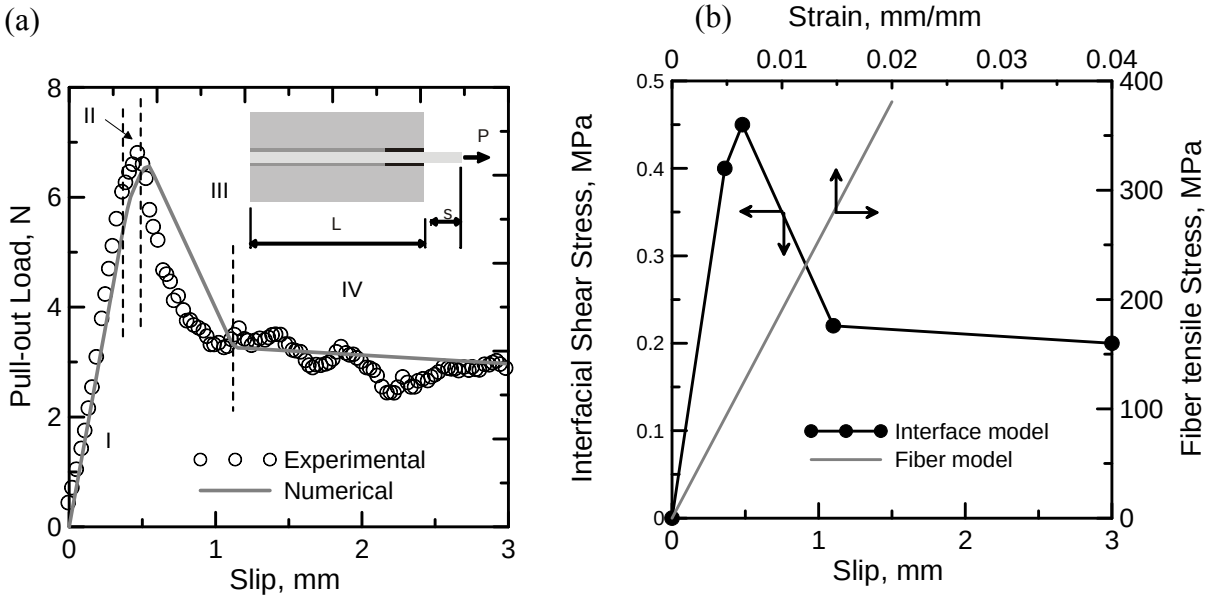

Fig. 4: Fiber pull out test results of a AR Glass (L=20 mm) Compared with numerical finite difference model and (b) Interface constitutive relation used in the finite difference simulation

The influence of the matrix first crack strength on the tensile and crack spacing is shown in Figure 5(b). Both the ultimate strain and crack spacing increase as the matrix first crack strength is increased ranging from 3.5 to 6.5 MPa. No effect on the ultimate tensile strength (UTS) is observed.

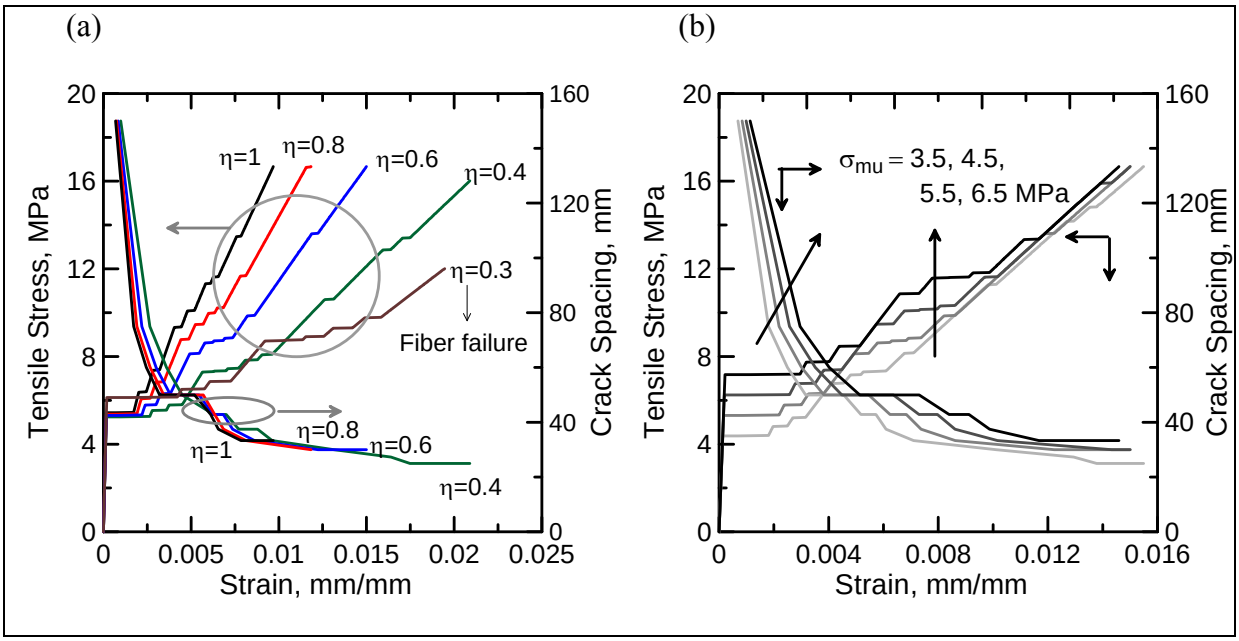

Fig. 5: Simulation of tensile response and crack spacing: a) effect of efficiency factor of fiber modulus and strength, and b) effect of matrix first crack strength. (the arrows point to the specific axis corresponding to the plots shown, or the range of variables used)

Figure 6 shows the comparison between experimental and predicted tension and cracking spacing behavior. It used an efficiency factor $\eta = 0.6$, matrix first crack strength of 7 MPa and the interfacial bond model presented in Figure 4b. The predicted stress-strain response also shows a good fit with experimental values therefore validating the used model. This verification has been done for the upper bound values and changing the variables will enable the fitting of the lower bound values as well. Note that the model correlates well with the upper bound experimental curves up to a strain of 1.0%. After that point it overestimates both the experimental curves. The predicted crack spacing response obtained from the tension stiffening model correlates well with the experimental results as shown in Figure 6 top portion, as the model accurately predicts the saturated crack spacing. The numerical crack spacing shows an accurate prediction up to a strain value of 0.005 %. At the crack saturation level, an approximate spacing of 30 mm is obtained using the model which compares to a 23 mm for experimental results.

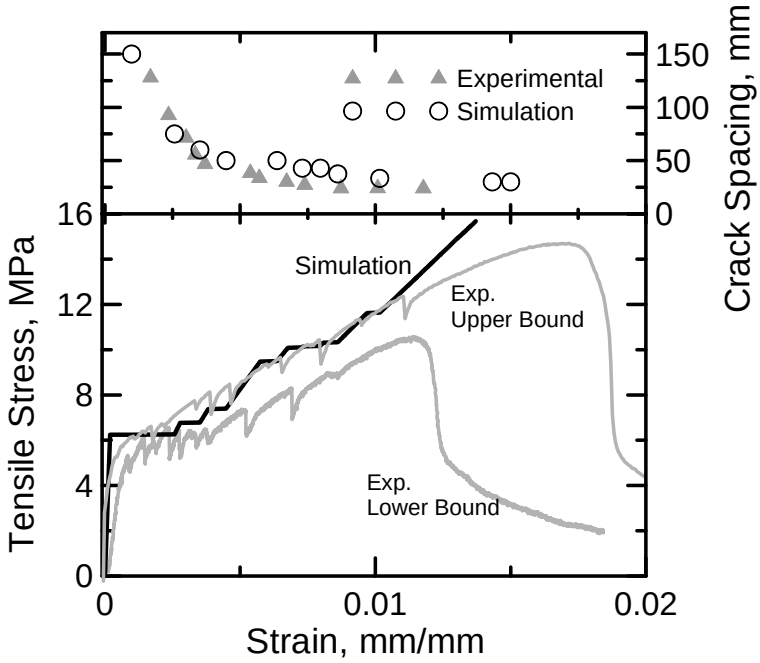

Fig. 6: Comparison of experimental and numerical results of the composite tensile response and crack spacing. Lower and upper bound experimental data compared with the numerical simulation [16].

2 Simplified Strain-Hardening Fiber Reinforced Concrete Model

A general strain hardening tensile, and an elastic perfectly plastic compression model as derived by Soranakom and Mobasher [17] and shown in Figure 7 is used to further simplify the tension stiffening model. Tensile response is defined by tensile stiffness, E, first crack tensile strain ε_{cr}, Cracking tensile strength, σ_{cr}, $=E\varepsilon_{cr}$, ultimate tensile capacity, ε_{peak}, and post crack modulus E_{cr}. The softening range is shown as a constant stress level $\mu E\varepsilon_{cr}$, and the compression response is defined by the compressive strength σ_{cy} defined as $\omega\gamma E\varepsilon_{cr}$. In order to simplify material characteristics of strain-hardening FRC, and yet obtain closed form design equation generation several assumptions are made. It has been shown that the difference in compressive and tensile modulus, parameter γ, has negligible effect to the ultimate moment capacity [17]. By defining all parameters as normalized with respect to minimum number of variables, closed form derivations are obtained. Applied tensile and compressive strains at bottom and top extreme layers (Fig. 7c), β, and λ are defined as:

$$\beta = \frac{\varepsilon_t}{\varepsilon_{cr}} \quad \lambda = \frac{\varepsilon_c}{\varepsilon_{cr}} \tag{1}$$

Material parameters required for the simplified models are summarized as follows. Parameters, α, μ, η, ω, are defined respectively as representing normalized, tensile strain at peak strength, post-crack modulus, compressive yield strain:

$$\alpha = \frac{\varepsilon_{peak}}{\varepsilon_{cr}}, \qquad \eta = \frac{E_{cr}}{E}, \qquad \omega = \frac{\sigma_{cy}}{E\varepsilon_{cr}} = \frac{\sigma_{cy}}{\sigma_{cr}} \tag{2}$$

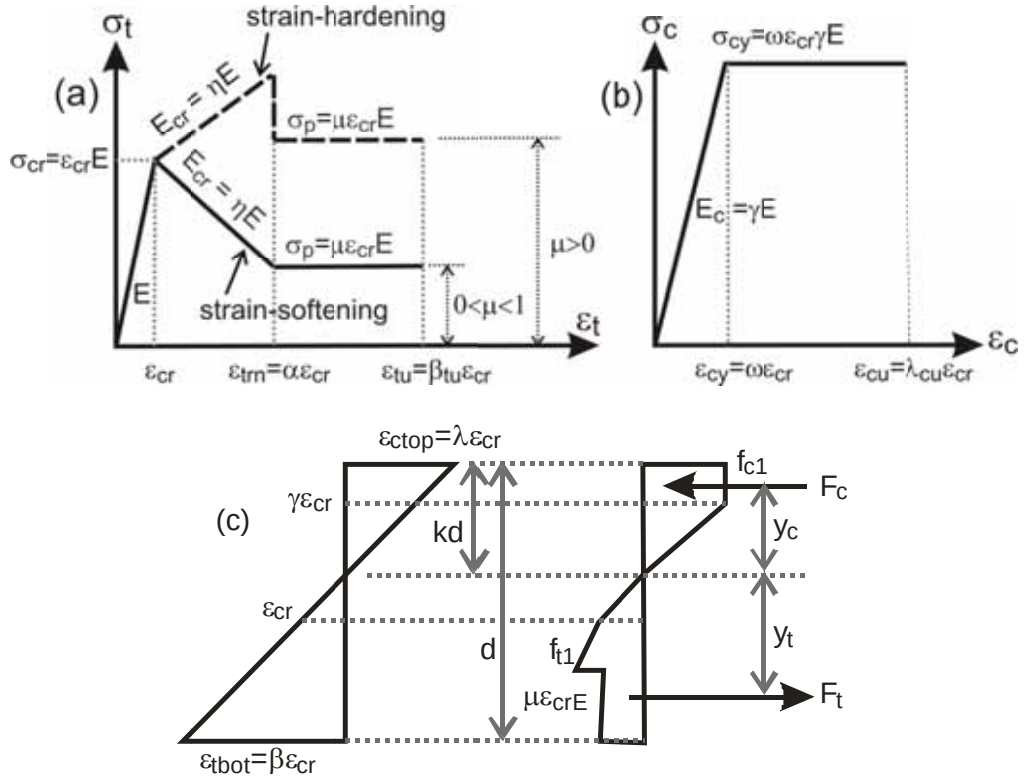

Fig. 7: Full option material models for both strain-hardening and strain-softening FRC: (a) tension model; (b) compression model, and (c) strain and stress disstribution across a cross section.

For typical strain-hardening FRC, the compressive strength is several times higher than the tensile strength. Thus, the flexural capacity is mostly controlled by the weaker tension component.

3 Derivation of Moment Capacity

Moment capacity of a beam section according to the imposed tensile strain at the bottom fiber ($\varepsilon_t = \beta\varepsilon_{cr}$) can be derived based on the assumed linear strain distribution. By using material models described in Figure 7(a)&(b), force components, their centroidal distance to the

neutral axis, the moment and curvature distributions are obtained. The depth of neutral axis, the nominal moment capacity M_n is obtained by taking the first moment of force about the neutral axis, is expressed as a product of the normalized nominal moment m_n and the cracking moment M_{cr}

$$M_n = m_n M_{cr} , \qquad M_{cr} = \frac{\sigma_{cr} b h^2}{6} \tag{3}$$

Location of neutral axis and moment capacity are obtained by the definitions provided in Table 1. This table presents all potential combinations for the interaction of tensile and compressive response. According to bilinear tension and elastic compression models shown in Figure 7(a)&(b), the maximum moment capacity is obtained when the normalized tensile strain at the bottom fiber ($\beta = \varepsilon_t/\varepsilon_{cr}$) reaches the tensile strain at peak strength ($\alpha = \varepsilon_{peak}/\varepsilon_{cr}$). Note that depending on the relationship among material parameters, any of the zones 2.1, and 2.2, or 3.1, and 3.2 as shown in Table 1 are potentially possible.

Analysis of these equations indicates that the contribution of fibers is mostly apparent in the post cracking tensile region, where the response continues to increase after cracking [Figure 7(a)]. The post-crack modulus E_{cr} is relatively flat with values of η = 0.00-0.4 for a majority of cement composites and can be directly related to the efficiency of the textile bonding mechanism discussed before. The tensile strain at peak strength ε_{peak} is relatively large compared to the cracking tensile strain ε_{cr} and may be as high as α = 100 for polymeric based fiber systems. These unique characteristics cause the flexural strength to continue to increase after cracking. Since typical strain-hardening FRC do not have a significant post-peak tensile strength, the flexural strength drops after passing the tensile strain at peak strength. Furthermore the effect of post crack tensile response parameter μ can be ignored for a simplified analysis. In the most simplistic way, one needs to determine two parameters in terms of post crack stiffness η, and post crack ultimate strain capacity α, to estimate the maximum moment capacity for the design purposes.

4 Analysis - Prediction of Load Deflection Response of Fabric Cement Composites

TRC composites that use a bonded AR glass, and reported earlier are used in the simulation phase [18]. These composites were manufactured using a cement paste with a water to cement ratio of 0.45, and AR glass fabrics manufactured by Nippon Electric Glasss Company. The AR Glass bundle had a Strength of 1360 MPa, a Modulus of elasticity of 78 Gpa, filament size of 13.5 microns and a bulk bundle diameter of 0.8 mm. The grid size was 4 yarns per cm with 2 individual yarns in each the longitudinal and transverse directions [18][19]. The textile reinforced composites had 8 layers of textiles.

Uniaxial tensile results of these composites 10x25x200 mm in dimension are shown in Figure 8a. The initial linear region terminates by cracking at the Bend over Point (BOP) and fol-

lowed by the formation of multiple cracking. As multiple cracking takes place, the stiffness of the sample significantly drops while the crack spacing decreases to about 20 mm reaching saturation crack spacing at this level. The saturation of crack spacing correlates to overall strain levels corresponding to 1.5%. [11,12]

In order to correlate the tension and bending responses, experimental data from a set of specimens under three point bending tests were also used. The flexural specimens were 10x25x200 mm with a clear span of 152 mm. Figure 8(b) shows the predicted flexural load deflection response of cement composites. The material parameters for tension model were determined by fitting the model to the uniaxial tension test and flexural test result as shown by the dashed line in Figures 8(a) and 8(b).

Stage	Parameters	k	$m = M/M_{cr}$
1	$0 < \beta \le 1$	$k_1 = \begin{cases} \frac{1}{2} & \text{for } \gamma=1 \\ \frac{-1+\sqrt{\gamma}}{-1+\gamma} & \text{for } \gamma \neq 1 \end{cases}$	$m_1 = \frac{2\beta\left[(\gamma-1)k_1^3 + 3k_1^2 - 3k_1 + 1\right]}{1-k_1}$
2.1	$1 < \beta \le \alpha$ $0 < \lambda \le \omega$	$k_{21} = \frac{D_{21} - \sqrt{D_{21}\gamma\beta^2}}{D_{21} - \gamma\beta^2}$ $D_{21} = \eta\left(\beta^2 - 2\beta + 1\right) + 2\beta - 1$	$M'_{21} = \frac{\left(2\gamma\beta^3 - C_{21}\right)k_{21}^3 + 3C_{21}k_{21}^2 - 3C_{21}k_{21} + C_{21}}{1-k_{21}}$ $C_{21} = \frac{(2\beta^3 - 3\beta^2 + 1)\eta + 3\beta^2 - 1}{\beta^2}$
2.2	$1 < \beta \le \alpha$ $\omega < \lambda \le \lambda_{cu}$	$k_{22} = \frac{D_{22}}{D_{22} + 2\omega\gamma\beta}$, $D_{22} = D_{21} + \gamma\omega^2$	$M'_{22} = \left(3\gamma\omega\beta^2 + C_{22}\right)k_{22}^2 - 2C_{22}k_{22} + C_{22}$ $C_{22} = C_{21} - \frac{\gamma\omega^3}{\beta^2}$
3.1	$\alpha < \beta \le \beta_{tu}$ $0 < \lambda \le \omega$	$k_{31} = \frac{D_{31} - \sqrt{D_{31}\gamma\beta^2}}{D_{31} - \gamma\beta^2}$ $D_{31} = \eta\left(\alpha^2 - 2\alpha + 1\right) + 2\mu(\beta - \alpha) + 2\alpha - 1$	$M'_{31} = \frac{\left(2\gamma\beta^3 - C_{31}\right)k_{31}^3 + 3C_{31}k_{31}^2 - 3C_{31}k_{31} + C_{31}}{1-k_{31}}$ $C_{31} = \frac{(2\alpha^3 - 3\alpha^2 + 1)\eta - 3\mu\left(\alpha^2 - \beta^2\right) + 3\alpha^2 - 1}{\beta^2}$
3.2	$\alpha < \beta \le \beta_{tu}$ $\omega < \lambda \le \lambda_{cu}$	$k_{32} = \frac{D_{32}}{D_{32} + 2\omega\gamma\beta}$, $D_{32} = D_{31} + \gamma\omega^2$	$M'_{32} = \left(3\gamma\omega\beta^2 + C_{32}\right)k_{32}^2 - 2C_{32}k_{32} + C_{32}$, $C_{32} = C_{31} - \frac{\gamma\omega^3}{\beta^2}$

$\phi = \phi'_i \phi_{cr}$ $\quad \phi'_i = \frac{\beta}{2(1-k_i)}$ Where i applies to cases in Table 1 referring to 2.1,2.2,3.1, and 3.2

Table 1: Neutral axis parameter k, normalized moment m and curvature ϕ for each stage of tensile strain at bottom fiber (β)

The steps in calculation of load-deflection response from the moment-curvature have been discussed in detail in recent publications dealing with strain hardening [20] and strain softening type composites [21, 22]. No attempt was made to obtain a best fit curve to the response. The average material properties for the simulation of upper bound values were: $\alpha = 65$, $\mu = 4$, $\eta = 0.06$, $\gamma = 5.0$, and, $\omega = 10$. The constants were $\varepsilon_{cr} = 0.0002$, and E = 20000 MPa, while the limits of the modeling were $\beta_{tu} = 135$, and $\lambda_{cu} = 40$. The material properties for the lower bound values were : $\alpha = 80$, $\mu = 3$, $\eta = 0.154$, $\gamma = 1$, and, $\omega = 10$. the constants were $\varepsilon_{cr} = 0.0008$, and E = 5200 MPa, while the limits of the modeling were $\beta_{tu} = 100$, and $\lambda_{cu} = 80$. Note that these values are shown for a preliminary set of data and proper optimization of the model with upper and lower bound values for each variable are required. It should also be mentioned that due to the nature of modeling a unique set of properties from the flexural tests can't be obtained and normally there are a set of tensile properties that may result in similar flexural responses. For this purpose it is essential to measure both tension and flexural responses together in the back-calculation processes.

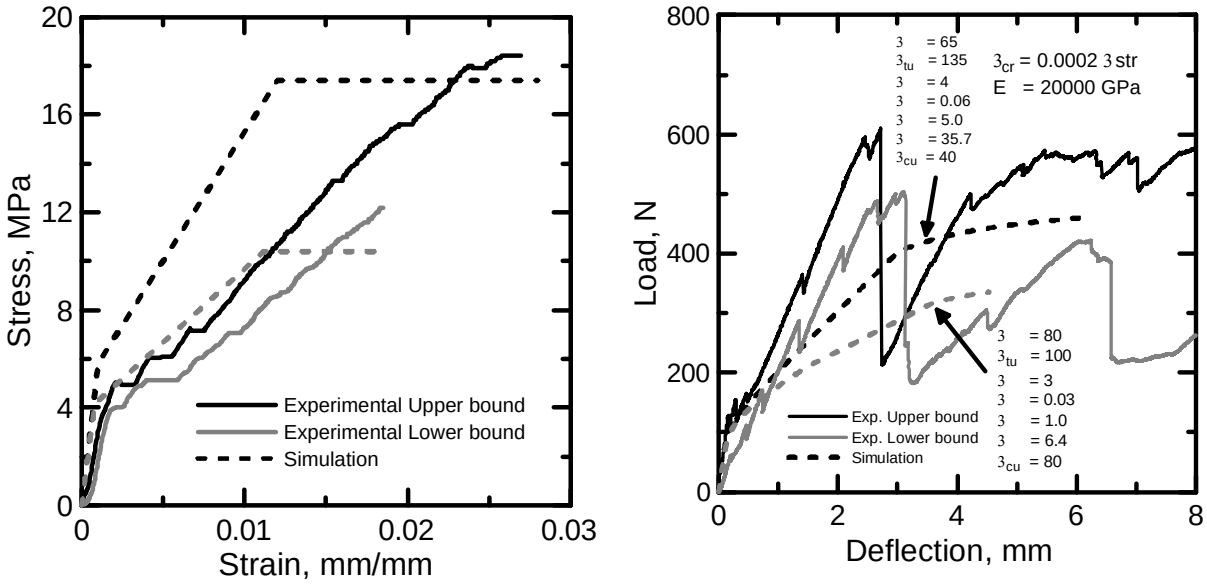

Fig. 8: Tensile stress strain response input model and predicted load deflection response of AR-Glass fabric composites.

In these systems, the high tensile stiffness and strength of the composite leads to high values for the load, and distributed flexural cracking. Analysis of the samples indicates formation of diagonal tension cracks in the samples due to the shear failure mechanism. No provisions for shear cracking were accounted for in the present approach.

Simulation that use direct tension data underestimates the equivalent flexural stress. This may be due to several factors including the size effect, uniformity in loading in tension vs. the

linear strain distribution in flexure, and variation in lamina orientation which may lead to a wider range of variation among the flexural samples. The underestimation of the flexural capacity can be eliminated by increasing the tensile capacity by scaling parameters as discussed in earlier publications, however these topics are beyond the scope of present work [17, 20, 22]. This procedure shows the potential for the use the flexural response and developing a reliable moment-curvature response that can be used for both back-calculation and also the design phase of the flexural load cases.

5 Design Guidelines- Simply supported Beam Under Distributed Load

The methodology used in the design of conventional reinforced concrete according to ACI-318 [23] is adopted next. The nominal moment capacity of a flexural member Mn must be decreased by a reduction factor to account for variability in materials and workmanships. The reduced capacity must be greater than the ultimate moment M_u due to factored loading by ACI Sec. 9.2.

$$\phi_r M_n \geq M_u \tag{4}$$

where ϕ_r is the reduction factor for strain-hardening FRC and may be conservatively taken as 0.8, equal to the reduction factor for compressive failure of plain concrete as stipulated by ACI Sec. C.3.5 [23] . Despite the post-crack flexural response of HPFRC is ductile such that it can sustain large deflections after cracking, it fails abruptly with little warning after passing the ultimate moment. For this reason, a conservative reduction factor for compressive failure of plain concrete is adopted. Flexural capacity of a simply supported beam subjected to a variety of loadings can be developed using standard approaches. For example, in the case of a distributed loading as shown in Figure 9, one can use the principal of virtual work to equate the external and internal work measures together. Application of yield line conditions while representing an upper bound approach is sufficiently conservative such that even when the full ultimate state safety factors are applied, the resulting failure modes are predictable and do not lead to catastrophic modes.

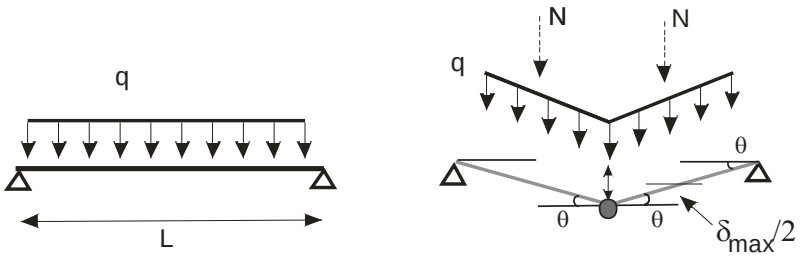

Fig. 9: The collapse mechanism in a flexural beam with distributed load.

Plastic analysis approach uses the principal of virtual work to equate the internal and external dissipated work to obtain the collapse load. For example for a distributed load on three point bend flexural beam as shown in Figure 9 , the work equations is derived as:

$$W_{int} = W_{ext} \qquad 2M_P\theta = 2M_P\left(\frac{2\delta}{L}\right) = 2[q\left(\frac{L}{2}\right)\left(\frac{\delta}{2}\right)] \qquad M_P = \frac{q_{ult}L^2}{8} \tag{5}$$

For a three point bending of a slab containing a single yield line along the centerline the collapse moment is computed in accordance to the following equation:

$$W_{int} = W_{ext} \qquad 2M_P\theta = P\delta = P\frac{L\theta}{2} \qquad M_P = \frac{P_{ult}L}{4} \tag{6}$$

This yield pattern can be used to define the potential collapse mechanism of a plate supported along its two or four edges. Flexural capacity of round slab simply supported subjected to a center-point loading is shown in Figure 11. Note that depending on the number of yield lines, the internal energy dissipation changes. It is however shown that in the case of simply supported round slab, the allowable applied load can be related to the bending moment capacity which is determined through laboratory tests on flexural samples.

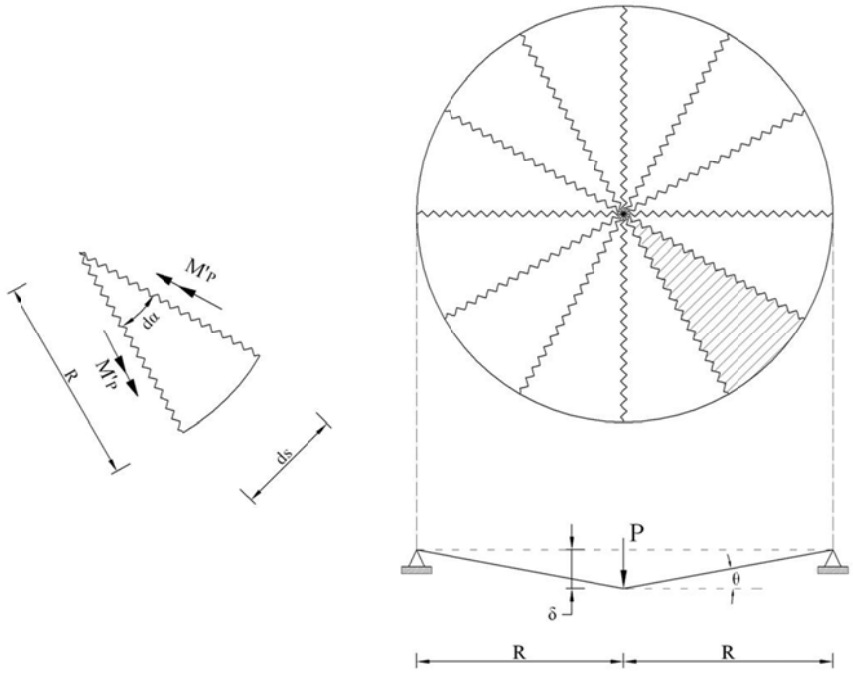

Fig. 10: Principle of virtual work used for the determination the ultimate load carrying capacity of a round panel test simply supported along its continuous edge, subjected to center point load.

$$W_{int} = W_{ext} \qquad \theta = \frac{\delta}{R} \qquad dW_{int} = M_P R\theta d\alpha = M_P \delta d\alpha$$

$$W_{int} = W_{ext} = \int_0^{2\pi} M_P \delta d\alpha = 2\pi M_P \delta = P_{ult}\delta$$

$$P_{ult} = 2\pi M_P \tag{7}$$

Using moment vs. allowable load relationship derived above in Eq 5, 6 and/or 7, one can obtain the required moment for a given applied load and depending on the cross sectional geometry and fiber type parameters allowed as design paramaters, determine the magnitude of variables and dimensions of test specimens to meet the ultimate moment capacity.

6 Conclusions

Procedures are presented to use a closed form solution based model as a basis for backcalcuation of tensile data from flexural samples. Using the same proposed methodology, one can compute the flexural capcity of strain hardening cement composites such as TRC materials. In order to expand the design implications, yield line theory can be used in conjunction with the model outputs to generate the ultimate moment capacity for a given geometry and loading conditions. The parametrized moment curvature response, once adjusted by the geometry and size of strain hardening material can be used to predict its moment capacity using principals of plastic design of structures or structural analysis software.

7 References

[1] HEGGER, J.; VOSS, S.: Investigations on the bearing behaviour and application potential of textile reinforced concrete," *Engineering Structures*, Volume 30, Issue 7, July 2008, Pages 2050-2056

[2] HEGGER, J.; WILL, N; BRUCKERMANN, O; VOSS, S: Load bearing behavior and Simulation of Textile Reinforced Concrete, Materials and Structures (RILEM), Volume 39, No. 8, Pages 765-776, 2006

[3] NAAMAN, A.E.; REINHARDT, H.W.: Setting the stage: toward performance based classification of FRC composites. In: *Proc of 4th Int workshop on High Performance Fiber Reinforced Cement Composites (HPFRCC-4), June 15-18, 2003, Ann Arbor, USA.* pp. 1–4.

[4] LI, V.C.: From micromechanics to structural engineering – the design of cementitious composites for civil engineering applications. *Struct Eng Earthquake Eng*, 10 (1994), p.1–34.

[5] NAAMAN, A.E.; REINHARDT, H.W.: Proposed classification of HPFRC composites based on their tensile response. *Mater Struct*, 39(289) (2006), p. 547–555.

[6] HEGGER,J.; M. HORSTMANN, J,; SCHOLZEN, A,: Sandwich panels with thin-walled textile reinforced concrete facings, ACI Fall Convention Puerto Rico, Published in ACI SP-251, 2007, pp. 109- 123.

[7] MOBASHER, B.; PAHILAJANI, J.; PELED, A.:Analytical Simulation of Tensile Response of Fabric Reinforced Cement Based Composites", *Journal of Cement and Concrete Composites*, Vol. 28, No. 1, Jan-2006, pp. 77-89.

[8] SUEKI, S.; SORANAKOM, C.; PELED, A.; MOBASHER, B.: "Pullout-slip response of fabrics embedded in a cement paste matrix, asce journal of materials engineering, vol. 19, 9, 2007.

[9] AVESTON, J.; COOPER, G.A.; KELLY, A.; The properties of fibre composites. In: *Conference Proceedings of the National Physical Laboratory*, Guildford : IPC Science and Technology Press Ltd., 1971, p. 15–26.

[10] SORANAKOM, C.; MOBASHER, B.: Geometrical and mechanical aspects of fabric bonding and pullout in cement composites. *Materials and Structures* 42 (2009), p. 765-777.

[11] SORANAKOM, C.; MOBASHER, B.: Modeling of tension stiffening in reinforced cement composites: Part I. Theoretical modeling, *Materials and Structures* 43 (2010), p. 1217-1230.

[12] SORANAKOM, C.; MOBASHER, B.: Modeling of tension stiffening in reinforced cement composites: Part II. Simulations vs. experimental results. *Materials and Structures* 43 (2010), p. 1231-1243

[13] SORANAKOM, C.: *Multi Scale Modeling Of Fiber And Fabric Reinforced Cement Based Composites.* Arizona State University, 2008-Dissertstion.

[14] BRAMESHUBER, W.: *State of the art report of RILEM Technical Committee,TC 201-TRC: Textile Reinforced Concrete*, 2006, 292.

[15] SUEKI, S.; SORANAKOM, C.; PELED, A.; MOBASHER, B.: Pullout–slip response of fabrics embedded in a cement paste matrix. *Journal of Materials in Civil Engineering* 19 (2007), p.178-727.

[16] SILVA, F.A.; ZHU, D.; MOBASHER, B.; SORANAKOM, C.; TOLEDO FILHO, R.D.: High speed tensile behavior of sisal fiber cement composites. *Materials Science and Engineering. A* 527 (2010), p. 544–552.

[17] SORANAKOM, C,; MOBASHER, B.: Correlation of tensile and flexural response of strain softening and strain hardening cement composites. *Cem. Concr. Compos.* 30 (2008), p. 465-477.

[18] PELED, A.; MOBASHER, B.: Pultruded fabric-cement composites. *ACI Materials Journal* 102(1) (2005), p. 15-23.

[19] MOBASHER, B.; PELED, A.; PAHILAJANI, J.: Distributed cracking and stiffness degradation in fabric-cement composites. *Materials and Structures* 39 (287) (2006), p. 317–331.

[20] SORANAKOM, C.; MOBASHER, B.: Closed-form moment-curvature expressions for momogenized fiber reinforced concrete. *ACI Material Journal* 104 (4) (2007), p. 351-9.

[21] SORANAKOM, C.; MOBASHER, B.; BANSAL, S.: Effect of material non-linearity on the flexural response of fiber reinforced concrete. IN: *Proceeding of the Eighth International Symposium on Brittle Matrix Composites BMC8, Warsaw, Poland*, 2006, pp. 85-98.

[22] SORANAKOM, C,; MOBASHER, B.: Closed form solutions for flexural response of fiber reinforced concrete beams. *Journal of Engineering Mechanics* 133 (8) (2007), p.933-41.

[23] ACI COMMITTEE 318. *Building Code Requirements for Structural Concrete. ACI Manual of Concrete Practice*, American Institute, Detroit, USA, 2005.